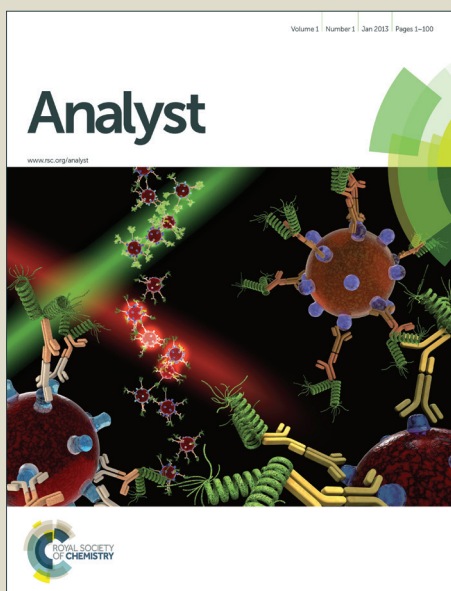


Analyst

Accepted Manuscript



This is an *Accepted Manuscript*, which has been through the Royal Society of Chemistry peer review process and has been accepted for publication.

Accepted Manuscripts are published online shortly after acceptance, before technical editing, formatting and proof reading. Using this free service, authors can make their results available to the community, in citable form, before we publish the edited article. We will replace this *Accepted Manuscript* with the edited and formatted *Advance Article* as soon as it is available.

You can find more information about *Accepted Manuscripts* in the [Information for Authors](#).

Please note that technical editing may introduce minor changes to the text and/or graphics, which may alter content. The journal's standard [Terms & Conditions](#) and the [Ethical guidelines](#) still apply. In no event shall the Royal Society of Chemistry be held responsible for any errors or omissions in this *Accepted Manuscript* or any consequences arising from the use of any information it contains.

ARTICLE

Exploring Copper Nanostructures as Highly Uniform and Reproducible Substrates for Plasmon-enhanced Fluorescence

Cite this: DOI: 10.1039/x0xx00000x

Received 00th January 2012,
Accepted 00th January 2012

DOI: 10.1039/x0xx00000x

www.rsc.org/

D. Volpati^{a,b*}, E. R. Spada^b, C.C. Plá Cid^c, M.L. Sartorelli^d, R.F. Aroca^e, C.J.L. Constantino^a

The unique property of metallic nanostructures of coinage metals that can sustain localized surface plasmon resonances (LSPR) put them at the centre of plasmon-enhanced phenomena. The theory for plasmonic phenomena based on LSPR is well-established. However, the fabrication of plasmonic substrates, reproducibly, is still challenging for applications in surface-enhanced Raman scattering (SERS) and surface-enhanced fluorescence (SEF). In this work we describe a well-ordered copper nanostructure (CuNS), produced by electrodeposition and nanosphere lithography, as active substrate for SEF. After a detailed spectroscopic and microscopic characterization, CuNS is successfully applied as SEF-active substrates using a well-known perylene derivative as target molecule. The signal reproducibility from CuNS substrates was established by comparing the results against those obtained from a simply roughened Cu substrate. For optimal conditions, signal variability is around 4%.

Introduction

Fluorescence-based detection techniques have a widespread use in areas of basic and applied life sciences, for being robust, highly-sensitive, specific and non-invasive. Finding new paths for fluorescence enhancement is therefore a key research area for genomics, proteomics, bioengineering, medical diagnostics, and industrial microbiology. Many strategies were already proposed, mostly based on the local electric field enhancement associated with localized surface plasmon resonances (LSPRs) of metallic surfaces, which is the key phenomenon for achieving surface-enhanced Raman scattering (SERS)^{1, 2}, surface-enhanced resonance Raman scattering (SERRS)³ and surface- or metal-enhanced fluorescence (SEF or MEF)^{4, 5}.

Despite the well-established theory for the surface-enhanced phenomena, the challenge exists of producing reliable and reproducible substrates with a predictable enhancement factor, which would allow one to add to the capabilities of SERS, SERRS and SEF as analytical tools⁶. Plasmonic substrates based on immobilization of metal nanoparticles have been extensively investigated, but these are inherently not reproducible, since there is no direct control over the formation of the metallic structures, which can vary from batch to batch⁷. Nanostructured substrates fabricated by electrodeposition through nanosphere lithography (ED-NSL)⁸ stand out as they allow a high throughput production of controlled periodic 2-D nanostructures with uniformity over large areas that is commercially viable. The surfaces generated by ED-NSL are particularly attractive

due to the possibility of excitation of different plasmonic modes either at the surface or confined to the spherical cavities⁹⁻¹¹. Different aspects in this line of research were already investigated that showed a rich interplay between plasmonic modes and their distinct effects on fluorescence or Raman intensities of fluorophores¹²⁻¹⁷. However, such studies concentrate on gold nanocavities^{14-16, 18, 19} and a strong emphasis is placed in the correlation between structure regularity and reproducibility^{14, 20}. Notably, other metals^{20, 21}, also, satisfy the requirements to support plasmon resonances in the UV-VIS region. Copper, in particular, has plasmonic properties similar to gold and silver³, it is less expensive; but it is prompt to oxidation in air¹⁷, which is detrimental for its use as plasmonic substrates, especially in case of nanoparticles²¹. However, this may not be the case for a continuous surface molded by NSL¹⁷. In addition for SEF (MEF), the spontaneously grown oxide layer may act as a spacer that prevents fluorescence quenching by the metal. In this work, we report a copper nanostructure (CuNS) produced by ED-NSL on Si substrates which is exposed to ambient conditions previous to its use as active substrate for SERRS and SEF. A highly uniform nine-fold enhancement factor for fluorescence is observed for a thin film of a perylene derivative deposited by physical vapor deposition onto the CuNS. The SERRS signal, though modest, was used as a probe of its high reproducibility. It is shown that the highest variability in signal intensity stems from defective regions located along the grain boundaries that separate regions of well-ordered domains. However, these fluctuations average out in a large area survey, achieving a

signal fluctuation of just 4%, which is comparable to the best substrates reported in literature^{7,20,22}.

Results and Discussion

CuNS and AzoPTCD films

The AzoPTCD film with a thickness of 10 nm was deposited simultaneously onto CuNS, roughened copper (CuR) and Si wafer. The latter is used as reference in the studies of enhancement factor (EF), which is estimated by comparing the intensities for AzoPTCD SEF from CuNS or from CuR and the intensity for AzoPTCD fluorescence from Si wafer. **Figure 1a** shows the architecture developed to support the CuNS or CuR (SEF) and the AzoPTCD film over Si wafer (reference fluorescence), which was fixed on a larger glass plate to facilitate sample manipulation. **Figure 1b** shows the UV-Vis absorption spectra for the 10 nm PVD film of AzoPTCD (black line), for CuNS (blue line) and for CuR (red line). It also shows the position of the excitation laser line, at 633 nm, in the spectral range studied. All spectra presented in Figure 1b are in an arbitrary “y” scale to allow a comparison between the samples concerning the maximum absorbance position. The CuNS and CuR spectra reveal essentially the absorbance of the Cu in a honeycomb-like nanostructure or simply in a roughened surface, presenting a broad absorption band starting around 700 nm towards high energy values, which is similar to other results, presented in the literature for Cu nanoparticles or roughened surfaces²³⁻²⁵. For a detailed discussion of the optical absorption and plasmonic modes supported by metallic films containing honeycomb-like nanostructures, we refer to Kelf *et al.*^{9,10}.

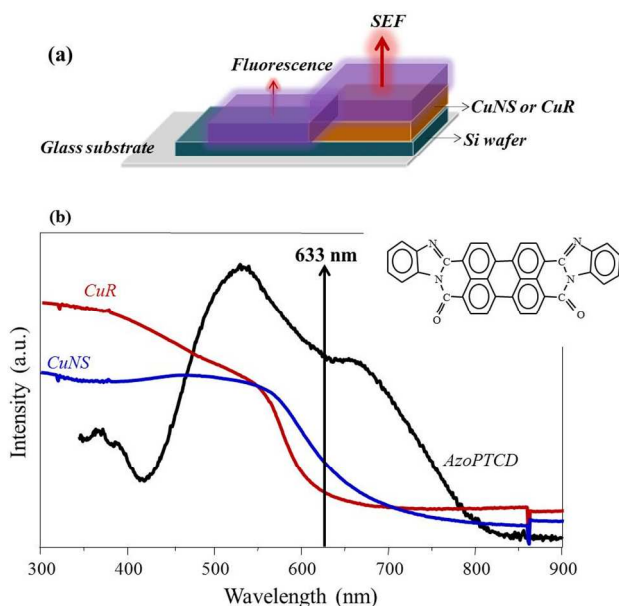


Figure 1: a) Design of the sample structure used to carry out the experiments; b) UV-Vis absorption spectra of 10 nm PVD film of AzoPTCD (black line), CuNS (blue line) and CuR (red line). Inset: structure of AzoPTCD (target molecule).

The electronic absorption of the AzoPTCD is already well known in the literature^{26,27}. The 10 nm PVD film of AzoPTCD

presents an intense blue-shift component with a broad maximum at 540 nm and a red-shift component at 670 nm compared to AzoPTCD solution spectrum (not shown – for more details see Volpati *et al.*²⁷). The strong red and blue-shift in the UV-Vis absorption spectra indicate an intermediate case of organized head-to-tail molecules described by Kasha's point dipole model²⁸, which results in the apparent band splitting, as observed for this perylene derivative and others²⁹. In addition, the 633 nm excitation laser line overlaps with a strong absorption of the CuNS film, leading to the resonance effect required to activate the surface-enhanced phenomena^{1,30}.

SEM image acquired by BSE mode was collected from the CuNS and can be seen in Figure 2a, showing the honeycomb-like arrangement. Likewise, Figure 2b shows a SEM image of the naturally roughened Cu; where it is clear the absence of an ordered structure. Figure 2a reveals that Cones is comprised of highly ordered domains 5-10 μm wide separated by defect lines or grain boundaries that are typical for colloidal masks formed by spin-coating. The method of nanosphere lithography has been previously used to fabricate SERS substrates. In the seminal work by Jensen *et al.*³¹ PVD was used in conjunction with a colloidal mask to deposit silver. The colloidal mask, in this case, has a screening effect that leads to an ordered array of triangular Ag islands. The method was later extended to the production of Cu islands over glass or silicon substrates³². Cintra¹⁸, Abdelsalam³² and co-workers, on the other hand, used electrodeposition to generate a continuous Au honeycomb structure similar to ours (more comparisons are made in the SERS discussion below). The main difference resides in the fact that the gold nanostructure is grown on top of a 200 nm Au thin film. In our work, the honeycomb copper grid has a direct interface with the underlying Si substrate, which is more similar to the geometry generated by Jose *et al.*¹⁴. For more detailed methods to produce active substrates for SERS, see, for instance, the review by Fan *et al.*⁶.

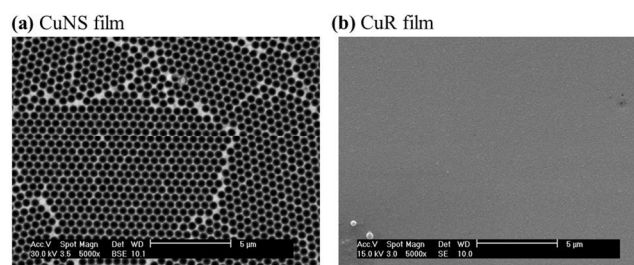


Figure 2: SEM images of a) CuNS revealing the honeycomb-like arrangement and b) Cu roughened.

AFM characterization of the CuNS, was carried out using contact mode in areas of 10 μm x 10 μm and 1 μm x 1 μm , which are presented in **Figure 3a** and **3b**, respectively. **Figure 3c** presents a profile (green line) extracted from the nanostructured surface shown in Figure 3b representing the holes formed after spheres removal, revealing a depth around 95 to 120 nm (Cu electrodeposition thickness) and a pitch around 500 nm (array periodicity). Other regions were analyzed and similar results were found. The same CuNS honeycomb-like arrangement was seen

(Figure 3a) and some statistical information could be extracted regarding the surface morphology. The first statistical information is the surface average roughness (R_a) extracted from the images using

the equation $R_a = \frac{1}{n} \sum_{i=1}^n |y_i|$. The second is the “root mean square”

roughness (R_{rms}) extracted from the data using the equation

$R_{rms} = \sqrt{\frac{1}{n} \sum_{i=1}^n y_i^2}$. For both equations “ y_i ” is each value

recorded by a punctual measurement and “ n ” is the number of points related to image resolution from where the values “ y_i ” were recorded. From a specific area of $4.0 \mu\text{m} \times 4.0 \mu\text{m}$ highlighted by the white square in Figure 3a, it was found a R_a of 17.1 nm and R_{rms} of 21.5 nm, and the maximum peak height was 142.7 nm. The same analysis was conducted for CuR nanostructures (Figure S1), and the results for R_a and R_{rms} were 11.4 nm and 14.2 nm, respectively, and the maximum peak height was 125 nm. These results reveal the advantages in producing patterned substrates at nanoscale yielding relative greater roughness and extended periodicity, essentials for the surface-enhanced phenomena.

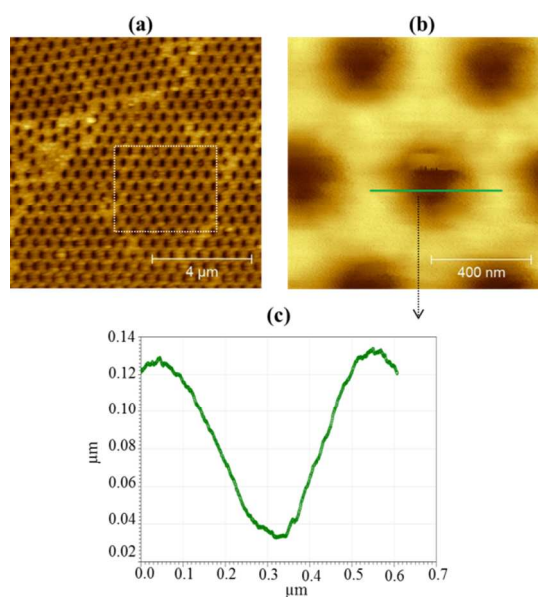


Figure 3. AFM images from a CuNS for distinct areas: a) $10 \mu\text{m} \times 10 \mu\text{m}$ and b) $1 \mu\text{m} \times 1 \mu\text{m}$. c) Profile extracted from the AFM image shown in (b) (green line).

Surface-Enhanced Fluorescence - SEF

The AzoPTCD was employed as target molecule to study the performance of CuNS as SEF active substrate. Figure 4 shows the emission spectra recorded using the 633 nm excitation laser line for 10 nm PVD film of AzoPTCD deposited onto Si wafer (fluorescence spectrum) and CuNS (SEF spectra). The figure S2 in supplementary information shows the SEF and SERRS for AzoPTCD deposited on the top of CuR substrate, which are identical of those spectra

observed in CuNS in terms of band positions, however different on the maximum intensity of scattering. The emission spectra (fluorescence or SEF) are characteristic of PTCd derivatives, i.e., a strong and broad band centered at 813 nm (12300 cm^{-1}) for the 10 nm PVD film on Si wafer and at 810 nm (12345 cm^{-1}) for the film on CuNS, which is attributed to the excimer emission³³. The very strong excimer emission is due to the formation of organized structures or molecular stacking in the 10 nm PVD AzoPTCD films, which requires the chromophores being arranged with parallel and overlapping ring systems, as observed for α -perylene crystals^{34, 35}.

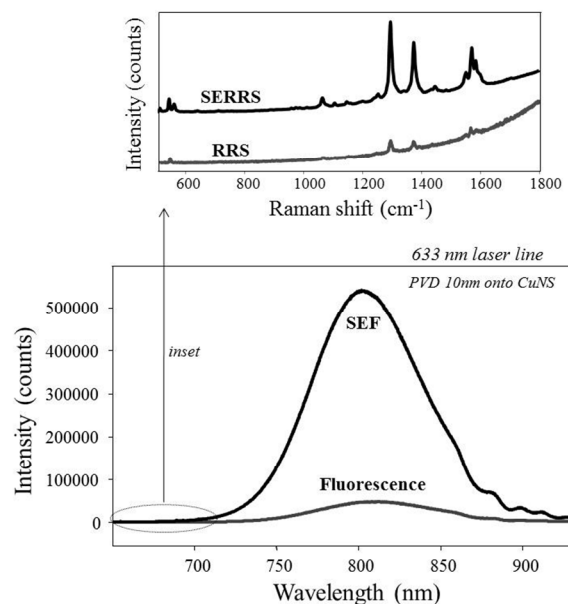


Figure 4: Fluorescence and SEF spectra recorded using 633 nm excitation laser line for 10 nm PVD film of AzoPTCD onto Si wafer and onto CuNS, respectively. Inset: RRS obtained for the AzoPTCD onto Si wafer and SERRS obtained for the AzoPTCD onto CuNS.

The possibility of recording fluorescence and SEF for the 10 nm PVD film of AzoPTCD on Si wafer and CuNS, respectively, allows estimating the enhancement factors (EF) considering the intensity ratios SEF/fluorescence, or $EF = \frac{I_{SEF}}{I_{Fluorescence}}$. The average EF found for SEF was around 9, keeping constant all the set up conditions. This values of EF is lower than that reported in previous work ($EF \sim 40$)²⁷ using 785 laser line and 10 nm AzoPTCD PVD films deposited over active substrates produced by 6 nm Ag evaporated films, which leads to nanostructured silver island films or SIF. The small EF found for SEF may be explained by the optical properties of the coinage metal used, since Cu has produced lower EF for surface enhanced phenomena when compared with Au and Ag. In addition, the oxide layer formed spontaneously on top of Cu nanostructures when in contact with air may not provide the optimum molecule-metal separation needed for SEF. The literature reports the formation of CuO and CuO₂ layers on the top of Cu thin films with 3.2 nm up to 4 nm of thickness^{17, 36}, which might not be the optimum distance between for fluorophore and metallic nanostructure studied here^{37, 38}. The observed values are consistent with the EF predicted by the electromagnetic mechanism, which

suggests SEF benefited from the enhanced local field and should be proportional to the square of the electric field with EFs commonly between 2 and 100 (much lower compared to SERS)^{4, 39}. However, the low reproducibility of SEF intensities from Ag islands, or other active substrates, at different regions of the substrate represents an obstacle to promising analytical applications⁶. The random distribution of size and shape of the Ag nanoparticles onto the substrate generates the variation on EF. On the other hand, the well-arranged CuNS honeycomb-like brings reproducibility on EF for SEF, as presented *vide infra*. The inset in Figure 4 shows a modest enhancement for RRS, but these SERRS spectra will be only used in this work to create reference Raman maps to monitor the reproducibility of the CuNS as an active substrate for surface-enhanced phenomena.

SEF – enhancement factors

The enhancement of the fluorescence from the AzoPTCD films deposited onto CuNS compared to AzoPTCD deposited onto Si wafer excited with 633 nm laser line is clearly seen in Figure 4. The EF was also investigated as a function of the incident laser power (633 nm) for the 10 nm PVD films of AzoPTCD deposited onto CuNS and CuR substrates, as shown in Figure 5a and 5b, respectively.

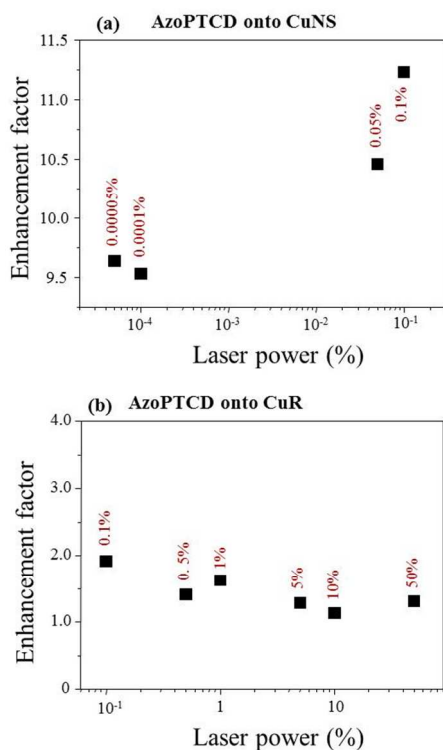


Figure 5: Enhancement factors (EF) estimated as a function of the incident laser power for (a) AzoPTCD onto CuNS and (b) AzoPTCD onto Cu roughened. 100% power = 1.25 mW.

In a direct comparison between the two sets of data, the CuNS presented EF values for SEF ca. ten times higher than those found for CuR. This is an experimental evidence of the role played by

designed nanostructures in the surface enhanced phenomena. Moreover, it is also possible to verify in Figure 5a a significant dependence of the EF on the excitation laser power (energy density at the sample), with a maximum EF for SEF found for a laser power of 0.1% of the incoming power (1.25 mW). The fluorescence enhancement of a fluorophore exhibits a maximum at a certain distance away from the surface^{4, 40, 41}. In a recent work⁴², we investigated the dependence of both fluorescence and SEF intensities with the power density of the exciting irradiation, and the results were attributed to a competition between excimer formation and photobleaching degradation in PTCd derivatives. This competition leads to the existence of a “maximum of emission” for a certain value of energy density exciting the sample⁴². However, the dependence observed here for EF on the incoming energy density seems to indicate that there is no competition between the rate of excimer formation and emission, and increased photobleaching of the PTCd moiety under plasmon enhanced resonance conditions.

CuNS – reproducibility study

The vibrational spectra of PTCd molecules have already been discussed for a series of other perylene derivatives⁴³. The SERRS spectra of the 10 nm PVD film of AzoPTCD deposited onto the CuNS (inset in Figure 4) were used as a tool to verify the reproducibility of the signal enhanced (SERRS signal) by the CuNS honeycomb-like structure. A detailed assignment of the characteristic vibrational normal modes of AzoPTCD is available in the literature²⁷. In order to monitor the SERRS signal reproducibility, the band at 1290 cm⁻¹ attributed to C-H bending + ring stretching (chromophore) was chosen to construct micro-Raman maps based on its intensity using a color scale, where the brighter spots refer to higher intensities.

As a first approach, a micro-Raman map was set up collecting spectra within the highly ordered regions, where each single point that belongs to the map was deliberately recorded in a specific region in the interior of the crystalline domains. Figure 6a shows an optical image of the 10 nm PVD film of AzoPTCD onto CuNS overlaid by a micro-Raman map (point-by-point) based on the intensity of the band at 1290 cm⁻¹ (color scale) from 25 spectra recorded in the interior of the grain. Figure 6b presents a 3D map containing all of 25 spectra mentioned in Figure 6a. The signal intensity fluctuates around 8,200 and 9,000 counts (< 10%), which is lower than other SERS active-substrates that have been used, such as PVD films (6 nm Ag islands, for instance)⁴⁴ or electrodeposited roughened electrodes⁴⁵.

Considering that the spatial resolution for these measurements is close to 1 μm², the fluctuation below 10% is acceptable. Abdelsalam *et al.*³² reported the use of Au to produce the same kind of honeycomb-like substrate for surface enhanced phenomena, and a fluctuation of 10% was reported for the signal intensity for 50 spectra collected randomly along benzene thiol dip-coating film adsorbed from 5 mM solution. Moreover, the authors mentioned that this kind of substrate is robust and stable, being used for more than 22 weeks.

A complementary experiment was carried out to appraise the role played by grain boundaries on the enhancement factor. **Figure 7a** shows an optical image of the 10 nm PVD film of AzoPTCD onto CuNS superposed by a micro-Raman map keeping the same experimental conditions used in the previous map, but now each one of the 25 spectra was purposely recorded along the grain boundary. **Figure 7b** shows a 3D micro-Raman map formed by the whole spectra recorded for each point shown in Figure 7a. The band intensity presents a fluctuation between ca. 7,000 and 10,000 counts (around 30%); evidencing an increase in EF variation, notwithstanding PTCF film homogeneity. So, it is reasonable to assume that the low ordered structure along the grain boundary (for more details see SEM images on Figure 2a) is responsible for the fluctuations of the SERRS signal intensity.

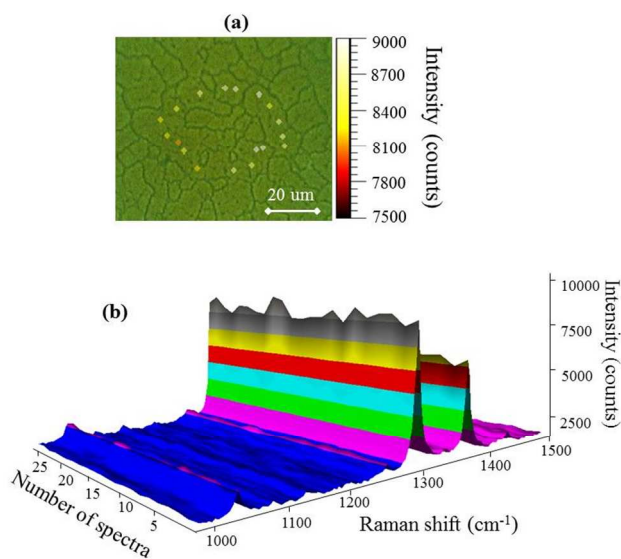


Figure 6: Micro-Raman maps formed by 25 spectra – a) two and b) three dimensions - for a 10 nm PVD film of AzoPTCD onto CuNS collecting spectra point-by-point on the interior of the grains. The two-dimensional Raman mapping is superposed to the optical image where the brighter spots refers to more intense signals for the band at 1290 cm^{-1} .

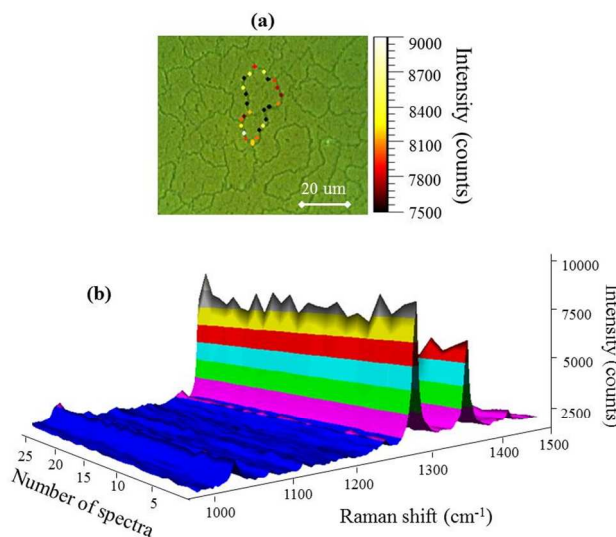


Figure 7: Micro-Raman maps formed by 25 spectra – a) two and b) three dimensions - for a 10 nm PVD film of AzoPTCD onto CuNS collecting spectra point-by-point along the grain boundary. The two-dimensional Raman mapping is superposed in an optical image where the brighter spots represent more intense signals for the band at 1290 cm^{-1} .

Based on the fact that grain boundaries may be responsible for the fluctuations of the signal, the equipment was set up to minimize these fluctuations even considering the grain boundary. The beam expander, an optical device that take a collimated light beam and expand its size, is used in the Raman equipment to control the laser focus (energy density) on the sample, where 0% indicates that the laser is tightly focused whereas 100% indicates it is completely defocused. Defocusing the laser beam reduces the energy density, and is frequently used to reduce damage in sensitive samples. The laser focus spot was opened from 0 to 100 % using the 50x lens, which provides a minimum laser spot about $1\text{ }\mu\text{m}^2$ when it is 0% opened and about 10 times larger when it is 100% opened. A microscope image of the sample CuNS with the laser focus 0% and 100% opened is depicted in **Figure S3** (Supplementary Information) for objective lens of 50x, illuminating the changes on the laser spot size. As we expected, the signal fluctuations were reduced to around 7%, making signal fluctuations smaller even for the spectra collected along the grain boundaries. An optimal condition was found by using the 5x objective lens and 100% of laser focus opened (results not shown), where the signal varied around 4%. This condition increases even more the surveyed area, since the 5x objective lens yields a laser spot about $35\text{ }\mu\text{m}^2$ when 0% of laser is opened. This new configuration made possible the acquisition of low-fluctuations spectra, resulting in significant improvement in terms of reproducibility.

Conclusion

The AzoPTCD film with 10 nm thick was used as a probe-fluorescent molecule to investigate the CuNS honeycomb-like structure as active substrate for surface enhanced phenomena, taking a Cu roughened film as a reference for the enhancement factor evaluation. In a direct comparison between the two types of Cu

substrate, the CuNS presented EF values for SEF ca. ten times higher than those found for CuR. This is an experimental evidence of the role played by designed nanostructures in the surface enhanced phenomena. The SERRS spectra were used as a tool to monitor the reproducibility of the signal enhanced by the CuNS. As a first approach, a micro-Raman map constructed collecting spectra in the inner part of the grain and the signal fluctuation observed was <10%, while for the data collected purposely along the grain boundary the fluctuation increased up to 30%. This fact evidenced the role played by the grain boundary on the SEF signal fluctuations. However, these fluctuations practically vanished from SEF spectra when the equipment is used with 5x objective lens (average SEF), confirming the successfully application of such active-substrates in the surface-enhanced phenomena.

Experimental Section

Copper substrates

All solvents and chemicals were of high quality. Copper and nickel sulfates and sodium citrate were purchased from Merck. Monodisperse polystyrene (PS) spheres, with nominal diameter of 535 nm, were obtained from Microparticles GmbH as 10 wt% aqueous solution. n-type (100) silicon wafers with 8-12 Ω .cm were used as substrates. Bi-distilled and deionized water (H_2O DD) were used in all fabrication steps.

For the preparation of CuNS, the silicon substrates (1.5 x 1.5 cm^2) were previously modified by a colloidal mask, as follows. First, a hydrophilic SiO_2 layer was grown on top of silicon: after 15 min sonication in water, the wafers were immersed in a solution of NH_4OH (25%) + H_2O_2 (40%) + H_2O DD, in a 1:1:5 ratio, for 1 hour at 82°C. The wafers were then thoroughly washed and kept immersed in water prior to use. 20 μ l of the PS colloidal solution were spin-coated over the Si surface, resulting in a highly uniform monolayered colloidal mask that was subsequently dried for a 24 h period at 60-70 °C.

Both CuR and CuNS were produced by direct Cu electrodeposition on Si, without the use of any seed layer, using the same electrolyte. The electrodeposition was performed with a PGSTAT302N potentiostat in a three electrode configuration, with a platin foil as counter-electrode and a saturated calomel electrode (SCE) as a reference. A circular electroactive area of 0.496 cm^2 , delimited by adhesive tape, was used as working electrode. The electrodeposition was performed from an electrolyte containing 0.019 mol dm^{-3} of $CuSO_4$, 0.170 mol dm^{-3} of $NiSO_4$ and 0.19 mol dm^{-3} of $Na_3C_6H_5O_7$. Prior to electrodeposition the silicon wafers with and without the colloidal mask were immersed in a 5% HF solution to remove the oxide layer. The potentiostatic deposition was performed at -0.6 V vs. SCE, where a preferential deposition of copper occurs (Figure S4). EDX measurements confirm the absence of Ni, indicating that if there are impurities of Ni it is below the detection limit of the equipment. In addition, the pattern of x-ray diffraction identified the fcc crystalline structure of Cu (Figure S4-b). The thickness of the metal was controlled by monitoring the charge passed during the electrodeposition process, and it was equivalent to 0.22 of the PS sphere diameter, which leads to a film thickness around 120 nm, for both types of Cu substrates.

In the case of CuNS, the polystyrene latex spheres were subsequently removed by dissolution in toluene for 5 minutes. The resulting structure and quality of the CuNS was confirmed using a scanning electron microscopy Phillips XL30 (SEM). The strict monolayered nature of the colloidal mask guarantees a film of homogeneous thickness⁴⁶.

Both CuR and CuNS were exposed to ambient conditions for two months before further use as plasmonic substrates.

PVD films of AzoPTCD

The sample of AzoPTCD was provided by Dr. J. Duff from Xerox Resource Centre of Canada. The PVD films of AzoPTCD were grown using the vacuum thermal evaporation technique in a Boc Edwards model Auto 306 machine. The growth process consists of placing the AzoPTCD powder in a metallic boat, where an electric current is passed through. The substrates (CuR and CuNS over Si wafers) were placed side-by-side and near (parallel) to the quartz crystal balance positioned 15 cm above the boat. The evaporation process was performed within a vacuum chamber under 10^{-7} Torr. The electric current was adjusted slowly from 0.0 up to 2.1 A (10V) to heat the boat until reaching the AzoPTCD evaporation temperature. When a constant evaporation rate around 0.5 nm/s is reached, the quartz crystal balance is zeroed and the shutter is opened allowing the growth of the PVD film until the desirable mass thickness.

Characterization techniques

The reflectance UV-Vis spectrum was measured using a tungsten-halogen lamp and the reflected light was collected using a Lambda 750 spectrophotometer. The wavelength used to illuminate the sample varied between 300 and 1000 nm. An integrating sphere was used to collect the signal, resulting in a precision of the order of 1 nm.

AFM measurements were carried out in a Nanosurf Easy Scan 2 microscope. Images with 10.0 x 10.0 μm^2 and 5.0 x 5.0 μm^2 were collected with resolution of 512 points/line using aluminum covered silicon probe in contact mode. The collected images and the statistical analyses were processed using Gwyddion software. The SEM images were taken with a Philips-XL30 scanning electron microscope (SEM) set for secondary electrons (SE) acquisition mode.

The Raman scattering spectra were collected using a micro-Raman Renishaw spectrograph, model in-Via, coupled to a Leica optical microscope equipped with 5x and 50x objectives lens leading to spatial resolutions from ca. 1 μm^2 to 50 μm^2 . The spectrograph is equipped with laser lines at 633 nm and gratings with 1200 and 1800 grooves/mm, leading to spectral resolution of ca. 4 cm^{-1} . Both extended and static measurements modes as well as different powers of the incoming laser (μW range) were used to improve the signal/noise ratio. Data acquisition and analysis were carried out using the WiRE software for windows and Galactic Industries GRAMS/32 C software.

Acknowledgements

The authors thank the Brazilian agencies CNPq (Process 143698/2008-7), CAPES, FAPESP (Processes 2011/11065-0 and 2012/09905-3), and the National Institute for Science and Technology on Organic Electronics (INEO) for financial support.

Notes and references

- a *D. Volpati**, C.J.L Constantino.
Faculdade de Ciências e Tecnologia, UNESP Univ Estadual Paulista, Presidente Prudente - SP, CEP 19060-900, Brazil.
*corresponding author: diogovolpati@gmail.com
- b *E.R. Spada, D. Volpati*
Instituto de Física de São Carlos, Universidade de São Paulo São Carlos/SP, 13560970 Brazil
- c *C. C. Plá Cid*
Laboratório Central de Microscopia Eletrônica, Universidade Federal de Santa Catarina
Florianópolis/SC 88040900 Brazil
- d *M. L. Sartorelli*
Departamento de Física, Universidade Federal de Santa Catarina
Florianópolis/SC 88040900 Brazil
- e *R..F. Aroca*
Materials and Surface Science Group, University of Windsor,
Windsor/On, N9B3P4, Canada.

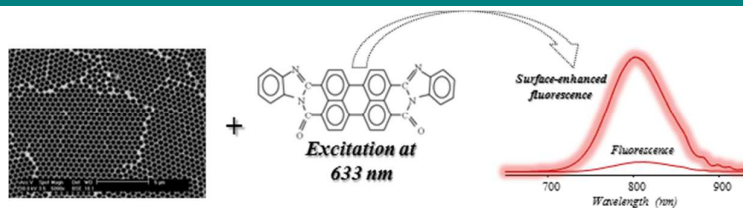
† Electronic Supplementary Information (ESI) available: [details of any supplementary information available should be included here]. See DOI: 10.1039/b000000x/

- M. Moskovits, *Rev Mod Phys*, 1985, **57**, 783-826.
- D. L. Jeanmaire and R. P. Van Duyne, *J Electroanal Chem Interfacial Electrochem*, 1977, **84**, 1-20.
- R. Aroca, *Surface-Enhanced Vibrational Spectroscopy*, John Wiley & Sons, 2006.
- A. Wokaun, H. P. Lutz, A. P. King, U. P. Wild and R. R. Ernst, *J Chem Phys*, 1983, **79**, 509-514.
- C. D. Geddes and J. R. Lakowicz, *J Fluoresc*, 2002, **12**, 121-129.
- M. K. Fan, G. F. S. Andrade and A. G. Brolo, *Anal Chim Acta*, 2011, **693**, 7-25.
- R. I. Nooney, O. Stranik, C. McDonagh and B. D. MacCraith, *Langmuir*, 2008, **24**, 11261-11267.
- P. N. Bartlett, J. J. Baumberg, P. R. Birkin, M. A. Ghanem and M. C. Netti, *Chem Mater*, 2002, **14**, 2199-2208.
- T. A. Kelf, Y. Sugawara, J. J. Baumberg, M. Abdelsalam and P. N. Bartlett, *Phys Rev Lett*, 2005, **95**, 1168021-1168024.
- T. A. Kelf, Y. Sugawara, R. M. Cole, J. J. Baumberg, M. E. Abdelsalam, S. Cintra, S. Mahajan, A. E. Russell and P. N. Bartlett, *Phys Rev B*, 2006, **74**, 24541501-24541512.
- R. M. Cole, J. J. Baumberg, F. J. Garcia de Abajo, S. Mahajan, M. Abdelsalam and P. N. Bartlett, *Nano Lett*, 2007, **7**, 2094-2100.
- F. Lordan, J. H. Rice, B. Jose, R. J. Forster and T. E. Keyes, *Appl Phys Lett*, 2010, **97**.
- B. Jose, C. T. Mallon, R. J. Forster and T. E. Keyes, *Phys Chem Chem Phys*, 2011, **13**, 14705-14714.
- B. Jose, R. Steffen, U. Neugebauer, E. Sheridan, R. Marthi, R. J. Forster and T. E. Keyes, *Phys Chem Chem Phys*, 2009, **11**, 10923-10933.
- P. N. Bartlett, J. J. Baumberg, S. Coyle and M. E. Abdelsalam, *Faraday Discuss*, 2004, **125**, 117-132.
- Y. Sugawara, T. A. Kelf, J. J. Baumberg, M. E. Abdelsalam and P. N. Bartlett, *Phys Rev Lett*, 2006, **97**, 2668081-2668084.
- I. Platzman, R. Brener, H. Haick and R. Tannenbaum, *J Phys Chem C*, 2008, **112**, 1101-1108.

- S. Cintra, M. E. Abdelsalam, P. N. Bartlett, J. J. Baumberg, T. A. Kelf, Y. Sugawara and A. E. Russell, *Faraday Discuss*, 2006, **132**, 191-199.
- F. Lordan, J. H. Rice, B. Jose, R. J. Forster and T. E. Keyes, *J Phys Chem C*, 2012, **116**, 1784-1788.
- S. Mahajan, J. J. Baumberg, A. E. Russell and P. N. Bartlett, *Phys Chem Chem Phys*, 2007, **9**, 6016-6020.
- J. H. Kim, S. H. Ehrman and T. A. Germer, *Appl Phys Lett*, 2004, **84**, 1278-1280.
- S. M. Wells, I. A. Merkulov, I. I. Kravchenko, N. V. Lavrik and M. J. Sepaniak, *Acs Nano*, 2012, **6**, 2948-2959.
- G. H. Chan, J. Zhao, E. M. Hicks, G. C. Schatz and R. P. Van Duyne, *Nano Lett*, 2007, **7**, 1947-1952.
- M. Epifani, G. De, A. Licciulli and L. Vasanelli, *J Mater Chem*, 2001, **11**, 3326-3332.
- P. F. Robusto and R. Braunstein, *Phys Status Solidi B*, 1981, **107**, 443-449.
- C. J. L. Constantino and R. F. Aroca, *J Raman Spectrosc*, 2000, **31**, 887-U883.
- D. Volpati, A. E. Job, R. F. Aroca and C. J. L. Constantino, *J Phys Chem B*, 2008, **112**, 3894-3902.
- V. Ramamurthy, *Photochemistry in Organized and Constrained Media Wiley-VCH*, 1991.
- P. A. Antunes, C. J. L. Constantino, R. F. Aroca and J. Duff, *Langmuir*, 2001, **17**, 2958-2964.
- K. Kneipp and H. Kneipp, *Appl Spectrosc.*, 2006, **60**, 322A-334A.
- T. R. Jensen, M. D. Malinsky, C. L. Haynes and R. P. Van Duyne, *J Phys Chem B*, 2000, **104**, 10549-10556.
- M. E. Abdelsalam, P. N. Bartlett, J. J. Baumberg, S. Cintra, T. A. Kelf and A. E. Russell, *Electrochem Commun*, 2005, **7**, 740-744.
- R. Hertmanowski, T. Martynski, R. Stolarski and D. Bauman, *Opto-Electron Rev*, 2008, **16**, 237-243.
- D. M. Donaldson, J. M. Robertson and J. G. White, *P Roy Soc Lond A Mat*, 1953, **220**, 311-321.
- J. Tanaka, *B Chem Soc Jpn*, 1963, **36**, 1237-1249.
- P. Keil, D. Lützenkirchen-Hecht and R. Frahm, *AIP Conference Proceedings X-Ray Absorption Fine Structure*, 2007, **882**, 490-492.
- J. R. Lakowicz, C. D. Geddes, I. Gryczynski, J. Malicka, Z. Gryczynski, K. Aslan, J. Lukomska, E. Matveeva, J. Zhang, R. Badugu and J. Huang, *J Fluoresc.*, 2004, **14**, 425-441
- K. Ray, R. Badugu, and J. R. Lakowicz, *Langmuir*, 2006, **22**, 8374-8378.
- P. Bharadwaj and L. Novotny, *Opt Express*, 2007, **15**, 14266-14274.
- R. Aroca, G. J. Kovacs, C. A. Jennings, R. O. Loutfy and P. S. Vincett, *Langmuir*, 1988, **4**, 518-521.
- P. A. Antunes, C. J. L. Constantino, R. Aroca and J. Duff, *Appl Spectrosc*, 2001, **55**, 1341-1346.
- D. Volpati, N. P. W. Pieczonka, A. A. Zanfolim, R. F. Aroca and C. J. L. Constantino, *Trends Appl Spectrosc*, 2009, **7**, 69 - 81.
- R. F. Aroca, C. J. L. Constantino and J. Duff, *Appl Spectrosc*, 2000, **54**, 1120-1125.
- R. F. Aroca and C. J. L. Constantino, *Langmuir*, 2000, **16**, 5425-5429.
- W. M. Carvalho, Jr., D. Volpati, V. A. Nunes Carvalho, R. F. Aroca, C. J. L. Constantino and F. L. Souza, *Chemphyschem*, 2013, **14**, 1871-1876.
- E. R. Spada, A. S. da Rocha, E. F. Jasinski, G. M. C. Pereira, L. N. Chavero, A. B. Oliveira, A. Azevedo and M. L. Sartorelli, *J Appl Phys*, 2008, **103**, 1143061-1143065.

RSCPublishing

Table of contents



D. Volpati, E. R. Spada, C.C. Plá Cid, M.L. Sartorelli, R.F. Aroca and C.J.L. Constantino*

Exploring Copper Nanostructures as highly uniform and reproducible substrates for Plasmon-enhanced Fluorescence

Towards reproducible and feasible large-area active substrates for the surface-enhanced phenomena, we report antidot copper nanostructures produced by electrodeposition and employed as an active substrate for surface-enhanced fluorescence (SEF), which exhibits a relative great enhancement factor and reproducible signals along the areas investigated.